Proceedings of ASME Turbo Expo 2011
GT2011
June 6-10, 2011, Vancouver, British Columbia, Canada

GT2011-46689

EFFECT OF NON-UNIFORM BLADE ROOT FRICTION AND STICKING ON DISK STRESSES

Harold R. Simmons, P.E.
Southwest Research Institute®
Mechanical Engineering Division
San Antonio, TX 78238
Email: harold.simmons@swri.org

Vishwas Iyengar, Ph.D.
Southwest Research Institute®
Mechanical Engineering Division
San Antonio, TX 78238
Email: vishwas.iyengar@swri.org

ABSTRACT

Stress levels predicted by conventional disk modeling assumptions are lower than expected to cause conventional creep or fatigue damage consistent with slot failures experienced in some compressor and turbine disks. It was suspected that disparate slot to slot friction at the blade root surface will result in sticking of some blade roots as the turbine is shut down while adjacent blades slip; the un-resisted stuck root would pry the steeples apart causing additional bending stress. Testing of a blade root/disk slot pair in a load frame found that the blade root will stick in place as imposed radial loads decrease. Simulation of blade root movement during shutdown indicates peak stress can increase by 20% or more depending on geometric factors. The slot stress only rises above its maximum speed condition on shutdown (at 80% Max Speed in the example case). This brief stress rise will not cause significant creep damage, but can shorten disk life based on low cycle fatigue or hold time fatigue damage.

NOTATIONS

ω = rotational velocity, rad/sec = 2 π N/60
N = Rotor speed (rpm)
ρ = Mass density of blade material
A_i = Incremental section blade areas including root and platform
r_i = radius of each blade element
υ = Angle of root bearing surface
ξ = Disk slot broach angle relative to engine axis
y = Effective width of contact surface
w = Rim width
Z = Number of blades
Pitch = 2 π r_2/Z
r_1 = Radius to mid-contact at root bearing surface
d_2 = Minimum Circumferential width of disk lug
r_2 = Radius to Minimum Circumferential width
F_L = CF load of disk lug or steeple
F_T = CF load of disk root tang
e_2 = Bending moment arm for F_N
e_3 = Bending moment arm for F_T
z = Height of disk tang in bending
x = Height of disk tang in shear
L_D= Lug twist arm = P sin ξ
Θ = torque at the neck of the disk lug
$\dot{m}$ = Air Mass flow rate
ΔT = Temperature difference across stage
Cp = Specific heat at constant pressure
L_b = Blade Length
L% = Fraction of blade length to gas load point
K = Stiffness of steeple + root in tangential direction
P = Normal (Bearing) Load
Q = Shear (Friction) Load
μ_{dyn} = Sliding coefficient of friction
μ_{st} = Static coefficient of friction
A_b, A_d = Effective Rim Area in compression
E_b, E_d = Modulus of Elasticity of blade and disk
I_b, I_d = Effective inertias of blade root and disk in bending
C_b, C_d = Bending coefficient for blade root and disk

INTRODUCTION

Two experiences are explored that lean toward the stick-slip mechanism as a source for additional stresses that contributed unexpected to disk failure. This mechanism also supports a cause for sparsely distributed cracks based on the variability of blade root friction. The first experience discussed is chronic failures of the third stage fan disk lugs of a high performance aircraft engine. The second experience is a power turbine disk failure of an aeroderivative engine in mechanical drive service occurring at about half of expected life.

A number of studies [1-4] have initiated to resolve a spate of fan disk failures initiating from the contact region of the blade attachment slot. These studies confirm that small cracks due to fretting can initiate HCF cracking in highly stressed attachments that experience a vibratory environment.

Davidson [1] concludes with fracture mechanics analysis to support HCF fractures initiating from fretting cracks in a aircraft fan disk. Fretting and galling are related wear mechanisms that are caused by small relative motions of contacting surfaces under load; evidence of both were found. Galling is a form of wear caused by micro-welding of surface aspirates under heavy loads that remove metal as the welds are broken by the relative sliding motions. These relatively large motions and high contact pressures are expected due to changes in rotor speed. It is suspected that if fretting cracks occur, then subsequent galling could erase its effect on HCF.

Fretting involves very small motions usually associated with vibration; oxidation often occurs and high contact pressures are not required. Chan, et al, [2] focused on identifying the necessary steps required to develop a probabilistic fracture mechanics-based methodology for treating high-cycle fretting fatigue in military engine disks. He incorporated high-frequency vibratory stress cycles due to stator wakes, flutter, and rotating stall into a composite mission profile containing mostly low-cycle stresses. Enright, et al [3] states that fretting fatigue is dominated by the fatigue crack growth phase and is strongly dependent on contact stress magnitude. Murthy, et al [4] recognizes that high contact stresses exist near the edges of normally flat contact surfaces.

These studies [1-4] have not explored the effects of a stick-slip mechanism causing the blade root to preferentially stick in some slots increasing both contact and bending stresses.

Aircraft Engine Experience

The specific engine failure investigated experienced one crack in 80 attachment surfaces (40 blades) in something less than 10,000 cycles. On some engines, failures have occurred in as little as 2000 cycles. These failures impair engine reliability and impact operational economics.

Fan blade attachments are usually designed as axial entry, single tooth dovetails aligned with the airfoil profile as shown in Figure 1. Cracks were found in the disk lug below the leading edge on the pressure (concave) side of the blade.

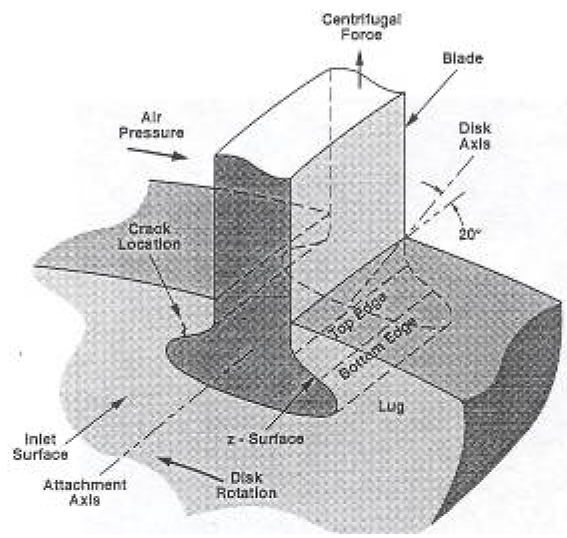

Figure 1 Axial Entry Dovetail Attachment Showing Disk Crack Location.

Metallurgical failure evaluation by Davidson [1] revealed heavy galling with 50 μm nearly uniform metal removal over the blade root contact surface; beveled edges occur where the contact runs out as shown in Figure 2. Wear marks appear as short 50–100 μm lines, spaced about 25 μm apart, aligned nearly perpendicular to the blade root axis, and parallel to the disk plane. The crack is located within the galled surface near the beveled edge as illustrated in Figure 3. It is reported that an anti-galling compound is used on some disks but was apparently displaced by repeated galling action.

Power Turbine Experience

The power turbine experience revealed nine cracks in one unit with 51 slots and only two cracks were in adjacent slots; only one fracture was observed on a second unit with no further crack indications; and a single crack in propagation was found on a third unit.

The rough blade root bearing surfaces found in Figure 4 appear as little oxide islands on both disk and blade surfaces that could interact to preferentially inhibit sliding; if true, static friction forces may be greater than expected. Blade root bearing stress (148 mPa) is well above 30 mPa galling threshold for most stainless materials; galling would increase the coefficient of friction. No substantial galling was found on the turbine disk, but in either case, it would be expected that coefficient of friction will increase with time and exposure.

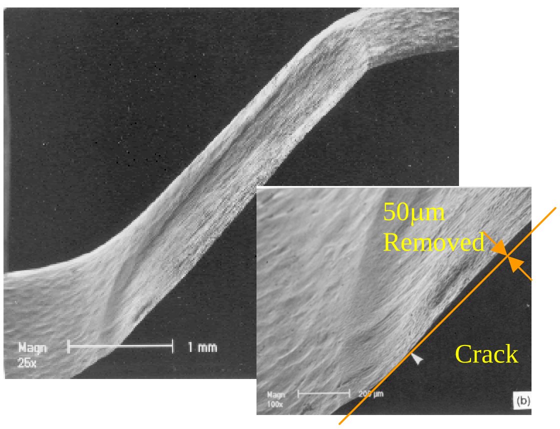

Figure 2 Oblique View of Disk Bearing Surface Showing the Extent of Wear. Crack Location is shown by the Arrow in the Inset.

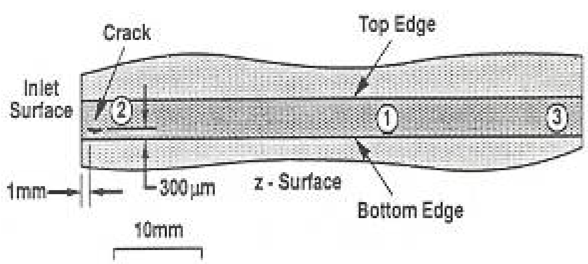

Figure 3 Crack Location within Blade Attachment Bearing Surface

BLADE ROOT STICK-SLIP

Disk stress analysis show that the blade roots slip outward as the disk expands with increasing speed; the root is pressed inward as the disk contracts with decreasing speed which increases bearing loads. Rudimentary simulation of this effect predict that loads and movements occur in jumps due to the difference in static and sliding friction; galling or oxidation should make slip occur with much greater jumps. It is not likely that friction will affect all blade roots uniformly, especially if some new blades are combined with refurbished blades as is common practice. Thus, one blade root may stick in place as the disk contracts while its neighbors slip. A blade root stuck in this way during shutdown will pry the disk steeples apart introducing bending stress at the fracture location.

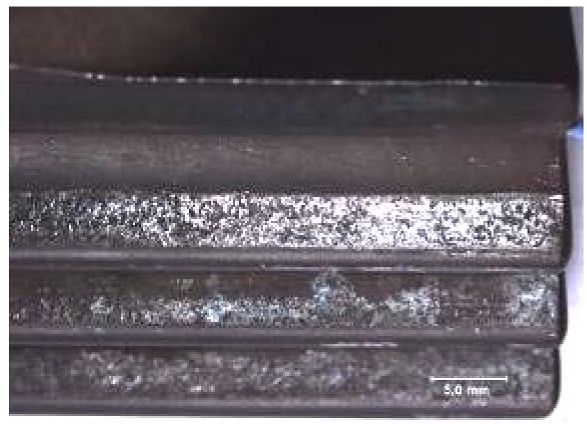

Figure 4 Blade Root Surface Roughness Suggest Increase Friction

The analyses of the disk lug and attachment surface, loading on the disk and blade are divided into three parts:

(1) Centrifugal loading due to rotor speed,
(2) Bending loads due to aerodynamic forces
(3) Transient forces and motions due to rotor acceleration/ deceleration

Centrifugal Loading

For many years before Finite Element Analysis (FEA) methods were available, fairly simple "Design Manual" equations were used in blade attachment design analysis to relate blade loading to root stresses. These equations served the design community with a consistent methodology to relate new engine design to prior experiences, both successful and non-successful. The experience base was applied across all blade attachments in fans, compressors, or turbines in advancing engine design.

The formulas and stress margins vary based on each manufacturer's philosophy and experience. The allowable stresses at critical locations, based on these equations, are a function of material properties, engine test cell results, and failures experienced.

The equations and nomenclature for blade root forces and stresses by Dundas [5], as given in the Sawyer Gas Turbine Handbook, is representative of a design manual approach and will be adapted herein. Dimension nomenclature is presented in Figure 5.

Centrifugal force created by each blade

$$F_B = \omega^2 \rho \sum_i A_i r_i \Delta r_i \qquad (1)$$

Where the summation includes elements of the airfoil, platform, and root

Normal force on each bearing surface

$$F_N := \frac{F_B \cdot \sec(\upsilon)}{2} \qquad (2)$$

Max bearing stress on tang

$$\sigma_{br} := \frac{F_N}{w \cdot y} \cdot \cos(\xi) \cdot \left(1 + 6 \cdot \pi \cdot \frac{r_1}{Z \cdot w} \cdot \sin(\xi)\right) \qquad (3)$$

Where the second term is due to unbalanced torque.

Tensile stress at disk lug minimum area

$$\sigma_t := \left(F_B + F_L\right) \cdot \frac{\cos(\xi)}{w \cdot d_2} \qquad (4)$$

Bending stress at disk tang

$$\sigma_b := 6 \cdot \frac{F_N \cdot \cos(\xi) \cdot e_2 + F_T \cdot e_3}{w \cdot z^2} \qquad (5)$$

Shear stress at disk tang

$$\tau := \frac{\frac{F_B}{2} + F_T}{w \cdot x} \qquad (6)$$

There is a torque (Θ) at the neck of the disk lug due to non-collinear forces of adjacent blades separated by the distance L_D as shown in Figure 5.

$$\Theta = \pi \frac{F_B}{Z} r_2 \tan(\upsilon) \sin(\xi) \qquad (7)$$

$$\tau_{Neck} = \Theta \frac{(3w + 1.8 d_2)}{w^2 d_2^2} \qquad (8)$$

Design allowable for blade root bearing stress is set fairly high (typically 60 – 80% of yield) based on the assumption that the first high stress cycle will cause yielding and a redistribution of stresses as the surfaces conform to one another. Sinclair and Cormier [8, 9] predict peak compressive stresses near the edges of the contact surfaces at about five times normal P/A stress; this is somewhat greater than yield thus, local plastic deformation is expected. Material removal due to galling should mitigate stress concentrations near the edges as the bearing surfaces become more conformal. All this presents a challenge for FEA modeling to include the uncertainties and changes in surface geometry that occur over time due to these mechanisms.

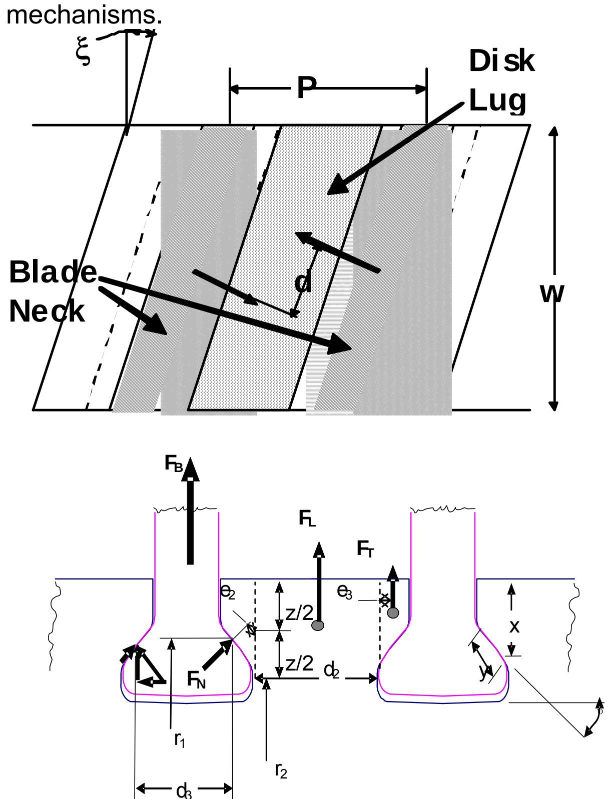

Figure 5 Dovetail Attachment Cross Section and Plan.

Gas Bending Loads

It is usually assumed that stress due to gas bending loads in compressor blading are minimal compared to centrifugal loading, however the high work per stage and length of fan blades suggests that gas loads may be significant as it is in the latter turbine stages.

Analysis of blade gas loading requires information on rated sea level static (SLS) mass flow, stage pressure ratio, and compressor inlet conditions at flight design points. While actual performance data may be restricted, reasonable estimates can be gleaned from published data (Janes[6]) on similar performance engines considering that gas loading is usually a minor effect. Estimates can always be revised if preliminary results show that gas loading is more significant compared to other loads.

Axial flow compressors (and fans) are actual volumetric flow machines; thus mass flow rate can be scaled by density for various flight conditions based on isentropic compression relationships for Mach number and altitude [7].

Fan blade loading is evaluated by a mean line flow analysis based on published fan pressure ratio of 3.125. A distribution of stage pressure ratios between 1.6 and 1.4 was assumed that resulted in the rated overall pressure ratio. Enthalpy rise per stage, based on pressure ratio, yields the conditions at the inlet and outlet of the third stage. High-performance trans-sonic airfoils are expected to have efficiencies in the 90 to 95% range.

Tangential blade loads are calculated from work per stage:

$$Wk_3 = \dot{m} C_p \Delta T \qquad (9)$$

Torque for the stage is

$$Tk_3 = Wk_3 / N \qquad (10)$$

Blade pressure loading is a function of lift, which varies along the span based on relative velocity, incidence, and camber. It is expected that lift will increase with radius but blade twist also increases to align with the incoming relative velocity vector. The net result tends to be compensating. Thus an average moment arm (L%) of 50% to 66% of airfoil span is usually chosen as the point to apply a representative gas load in the tangential direction.

$$F_b = \frac{Tk_3}{Z(L_b L\%)} \qquad (11)$$

Bending moment at the base of the blade root center is:

$$M_b = F_b\,(L_b\,L\%) \qquad (12)$$

Where L_b is the distance from airfoil base to midway on the root bearing surface

Bearing surface normal loads due to aerodynamic forces are calculated from geometric relationships assuming zero friction,

$$F_{bs} := \frac{M_b \cdot \sin(\zeta)}{G_r} \qquad (13)$$

These loads add to F_n; summing on the pressure side of the blade and subtracting on the suction side. Max load conditions are likely at flight envelope extremes of sea level ram or max Mach number at minimum altitude. Minimum loading conditions to consider are subsonic cruise (Mach = 0.8) and station keeping (Mach = 0.2).

Typically, fan blades have vibration snubbers in the form of integral part span shrouds that provide dynamic stiffening and damping. The shrouds are set roughly normal to the blade cord angle and provide static restraint in the torsional direction of the blade. As these shrouds are pre-loaded against one another, they provide some static restraint to bending forces in the axial and tangential directions up to the limit of friction. The friction restraint will reduce as a result of vibration and expansion of shroud ring due to CF loading and the unrestrained load condition will be approached. To avoid a nearly intractable calculation it is conservative to ignore shroud restraints for steady bending loads.

Transient Effects

The outer edge, or rim, of the disk is cut to form the blade attachment slots and does not support tangential (hoop) stresses. Centrifugal forces exerted on the disk as rotational speed increases cause the slot width to increase, which allows the blade to slip outward slightly. This slippage between the airfoil and disk surfaces is the major cause of galling damage.

A sum and difference approach attributed to Timoshenko & Goodier [10] for calculation of disk stress profiles is provided by Dundas [5]. This equation set, typical of early design practice, provides a simplified numeric approach that was applied in hand calculated spreadsheets to stimulate the speed and load transient effects. Figure 6 presents the hoop and radial stress profile at 10,400 rpm for a simplified version of the disk supporting the third stage blades; these stresses are functions of speed squared. The growth of slot width is base on hoop strain and the number of blades.

$$\Delta d_2 = E\,\sigma\,\pi\,r_2 / Z \qquad (14)$$

Temperatures in the fan section of the engine changes from 90° to 340°C during flight, and gradients between blade and disk will affect rim growth. If it is assumed that no more than 10°C differential will occur under extreme aircraft acceleration then thermal slot growth should be limited to 0.0023 mm which results in a band of slot growth uncertainty with speed as shown in Figure 7. It should be remembered that the thermal effect is transient and slot growth will return to the steady state curve.

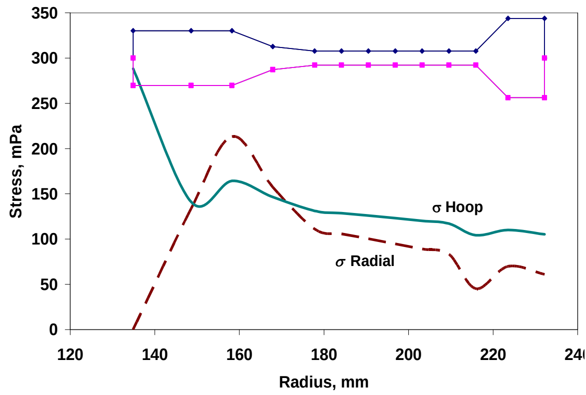

Figure 6 Disk Stress Profile at 10,400 rpm

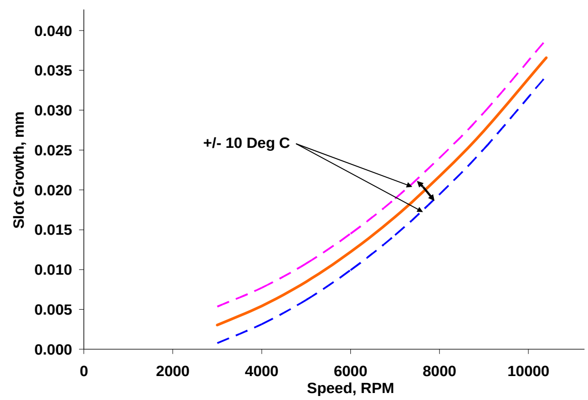

Figure 7 Slot Growth vs. Speed

The resulting slippage of the blade as the disk slot opens and closes is illustrated by the models in Figures 8 and 9. The forces on the attachment surface, which are both normal and sliding, are altered by the movement of the blade because of the tangential compliance and the friction between the two. The upper left part of Figure 8 illustrates the relation of tangential and radial blade root force vectors acting on the disk slot surface normal and sliding forces (P and Q) for the case of a closing disk slot; these forces are defined in equations 15 and 16.

$$P = F_{rad} / (\cos \varphi + \mu_{dyn} \sin \varphi) \qquad (15)$$

$$Q = \mu_{dyn} F_{rad} / (\cos \varphi + \mu_{dyn} \sin \varphi) \qquad (16)$$

Where radial force is ½ blade acting on ½ side of retaining lugs:

$$F_{rad} = m\, r\, \omega^2/2 \qquad (17)$$

$$Q = P\, \mu_{dyn} \text{ when in slip} \qquad (18)$$

$$Q \le P\, \mu_{st} \text{ when in stick} \qquad (19)$$

The disk slot expands in response to tangential forces (F_{tan}) acting on tangential stiffness (K) as well as imposed strain (Equation 14).

$$\Delta d_2 = E\, \Delta\sigma\, \pi\, r_2 / Z + \Delta F_{tan}/K \qquad (20)$$

Figure 9 illustrates the motions of the blade as compressive effects act on the disk and blade root components with tangential compliance.

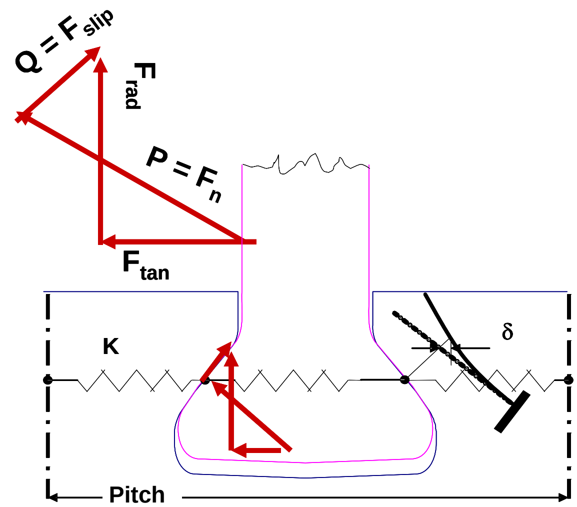

Figure 8 Blade Root Model with Tangential Compliance

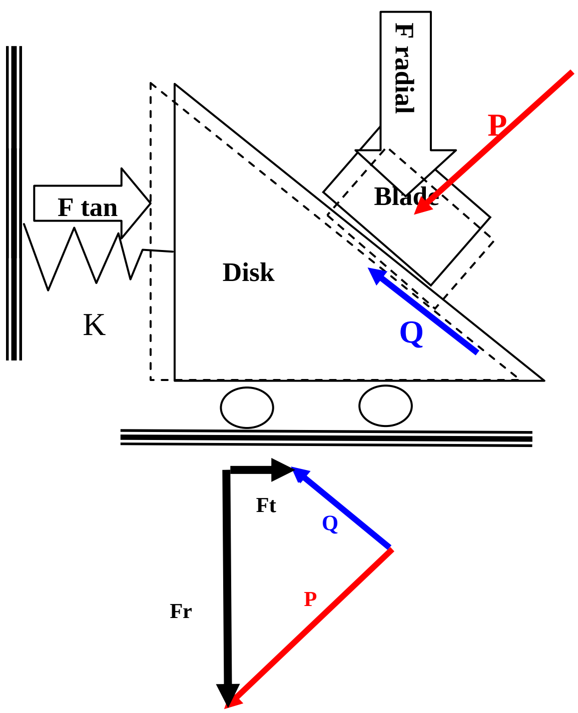

Figure 9 Blade Root/Disk Slot Model and Vector Diagram

Tangential stiffness (K) can be calculated by numerical models or estimated from the compressive effects of the disk lug and blade root section plus the bending deflection of the disk steeple and blade root. The disk lug and blade root are essentially wedge-shaped cantilever beams with distributed loads which exert bending forces at that reduce tangential stiffness.

$$\frac{1}{K} = \frac{d_2}{A_b E_b} + \frac{d_3}{A_d E_d} + C\frac{(y/2)^3}{E_b I_b} + C\frac{(y/2)^3}{E_d I_d} \quad (21)$$

A simple blade root/disk slot model shown in Figure 9 and Equations 14-20 was derived to predict sliding and static friction forces for both increasing and decreasing load trends. The simulation of a startup/shutdown would start about ¼ peak speed; the contact surface is assumed to be in equilibrium with no slippage and no unbalanced shear forces for the initial slot growth. Loads are calculated by equations 15, 16 and 17. The speed is incremented upward by a small fraction ΔN and slot growth calculated by Equation 20. P and Q are calculated for the "stick" assumption (Equations 15 & 16) and Q is compared with Q_{limit}.

$Q_{limit} = P\ \mu_{stick}$ (22)

If $Q_{stick} > Q_{limit}$ then

$F_{tan} = P \sin(\upsilon) - Q_{slip} \cos(\upsilon) - K\ \Delta d_2$ (23)

If $Q_{stick} < Q_{limit}$ then the previous calculated value is used for F_{tan}. With sufficiently small speed increments, the stair step stick slip displacements occur as shown in Figure 10.

Starting at the displacement position at maximum speed, speed is incremented downward with similar small steps. The stick-slip steps on descending speeds are predicted to be much greater than on ascending speed trends as shown in Figure 10.

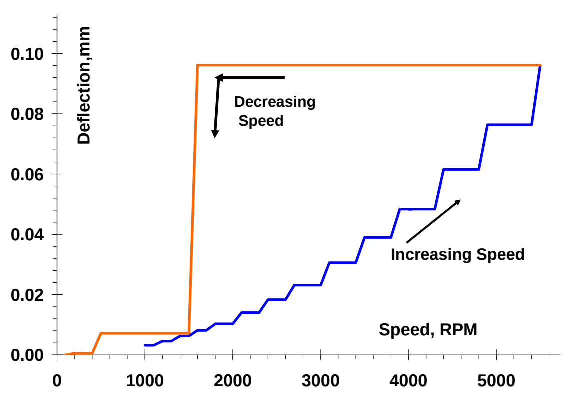

Figure 10 Deflection with Static & Sliding Friction Coefficients = 0.6 & 0.4

The stick-slip regime threshold is controlled by the static and sliding coefficients of friction and effective lateral stiffness of disk steeples which are all unknown prior to testing. Figure 11 illustrates the threshold trends for increasing and decreasing loads as a function of sliding friction for an assumed 700,000 kN/m steeple stiffness of. As can be seen, relatively small differences between static and sliding friction coefficients will allow stick-slip behavior and increasing this difference will increase the stick-slip effect.

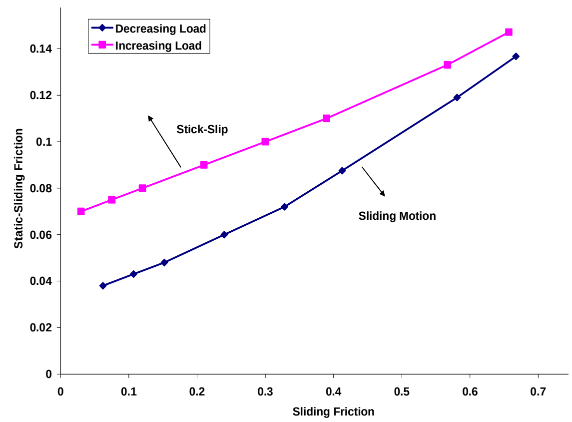

Figure 11 Stick-Slip Threshold of Static vs. Sliding Friction; K=700,000 kN/m

Stick-slip is more likely to occur with decreasing load trends than with increasing loads albeit the difference between the two is not great. Increasing steeple stiffness tends to raise the static friction required to cause stick-slip motion; a 50% rise in stiffness, for example, requires relative static friction increase of 25% and 40% for decreasing and increasing load trends respectively.

BLADE ROOT TESTING

A test was set up to characterize the mechanical friction response of a turbine blade and disk root attachment assembly at SwRI. The mechanical response of a turbine blade/disk assembly was evaluated under axial loading and integrated transducers (strain gages and linear displacement transducers). The main components of this test hardware are shown in Figure 12 and 13. Testing was exploratory at the start and the procedures were adapted to change based on initial results.

Testing was with the middle blade inserted as shown in Figure 13. Loading was in displacement control at 0.254 mm/min and load feedback was watched for non-linear behavior. The target load was near 180 kN but achieving that load was uncertain because the test specimen was fabricated from a blade that had experienced a failure. The operators were instructed to watch the load feedback for signs for yielding or significant change in the load response.

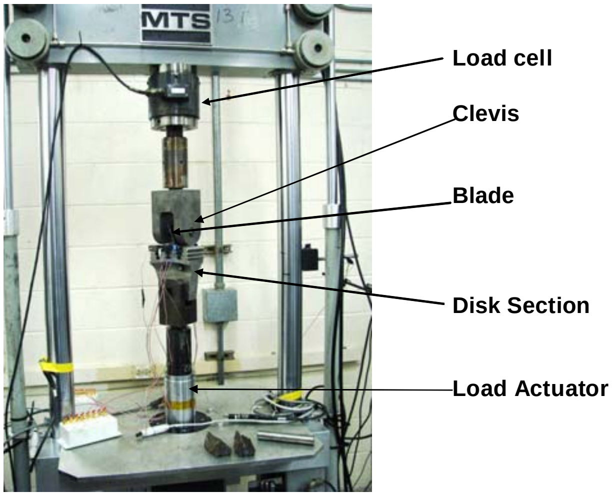

Figure 12 Blade Root/Disk Slot Pair in 50 Kips MTS Load Frame

A blade/disk root pair was tested in a MTS load frame. Measurements include load, total frame extension, strain at six locations including the failure location between steeples, and lateral extension of the steeples relative to each other. Load was slowly increased up to a maximum point; the load was paused at 22 kN increments to assess the prospect for significant differences in static and dynamic friction. Once the test item reach maximum load it was allowed to decrease.

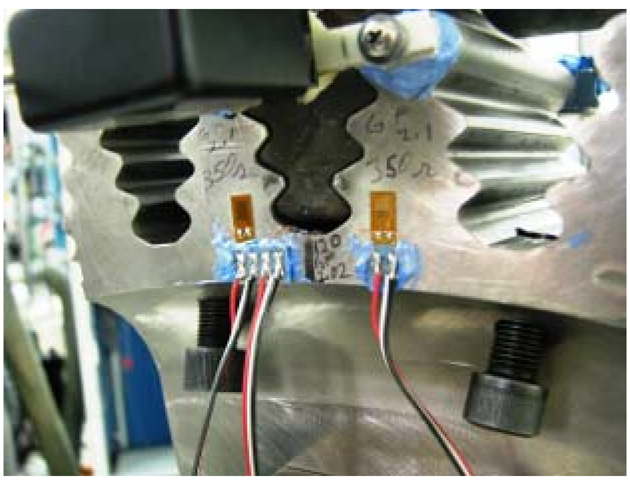

Figure 13 Typical Strain Gauge and Lateral Extensometer

Test Results

A typical Stress/Load plot is shown in Figure 14. The most dominant stress components are those measured in the slot at the failure location. The others traces are at locations where stresses are also expected to be relatively high.

Testing of a blade root/disk slot pair in the load frame found that the blade root will stick in place as imposed loads reduce such as when the unit speed decreases. Blade Root friction tests revealed much lower friction coefficients than expected.

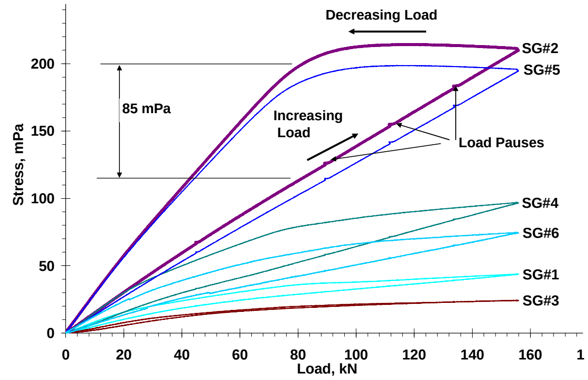

Figure 14 Typical Stress vs. Load Trace for Blade Root/Disk Slot Pair

The test results indicate the following findings about the stick-slip behavior of the blade root/disk steeple pair:

- The constant slope line from zero to maximum load indicates smooth sliding motion during the increasing load trend.
- Stress rises seen after each load pause is small, indicating small differences between static and sliding friction.
- Stress remains constant as load reduces to about 62% and then transitions to a constant declining slope that is different from load increase slope.
- This indicates the blade root sticks in place on initial load reduction and then slides smoothly with a different coefficient of friction than during increasing load.
- The maximum stress difference between increasing and decreasing load of about 85 mPa occurring near the transition point.

The blade root/disk slot model is compared with the deflection test data in Figure 15; steeple stiffness and friction coefficients are adjusted until the ascending load trend remains in sliding motion and the descending trends indicates a slip at 62% of max load. As can be seen the model is a poor match for the data, especially after the first descending load slip. It is likely that a partial slip model such as derived by Murthy [4] would more faithfully follow the descending trend however, it may not be necessary to simulate behavior at lower loads because the stress will have reduced to much less significant values. Table 1 presents the best fit friction and stiffness valves deduced from this exercise.

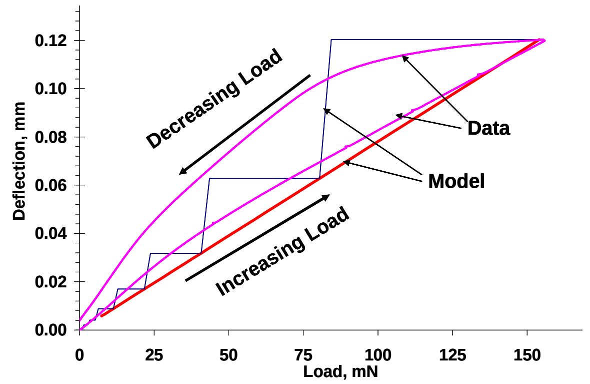

Figure 15 Comparison of Adjusted Stick-Slip Root Model with Deflection Test Results for K= 500000, mu = 0.15, 0.08

Table 1 Resultant Steeple Stiffness and Coefficients of Friction

K, kN/m =	**940,000**
μ Static =	**0.15**
μ Slip =	**0.08**

The stress measured is caused by tangential deflection of the steeples due to the tangential load components. A plot of measured slot stress vs. steeple deflection, as shown in Figure 16, indicates a slightly non-linear relationship between these two measurements; the nonlinear effect is probably due to the increasing moment as the blade root contact moves further out along the steeple and interacts with different bearing lands on the multiple landed root. The ascending trend of the data was fitted with a second degree polynomial as shown in the Figure. The effect of one blade root sticking in place while adjacent blades slip was simulated by summing the differential effect of the descending trend minus the ascending trend from the equation plus the hoop stress from the disk FEA analysis.

This simulation in Figure 17 shows that the blade root sticks until radial load reduces to 62% of its peak value, total stress at the failure location as calculated from the combined test data and FEA results reach a peak of almost 420 kN or 20% greater than the FEA hoop stress alone.

It should be noted that while this additional stress is dependent on the actual friction experienced in operation, which could be greater than the specimen tested, its peak would only be expected when the turbine speed decreases to about 80% of normal operating speed. Thus, this friction effect will not affect creep-rupture time because its effect is short lived; this stress spike will affect LCF or Hold-Time fatigue.

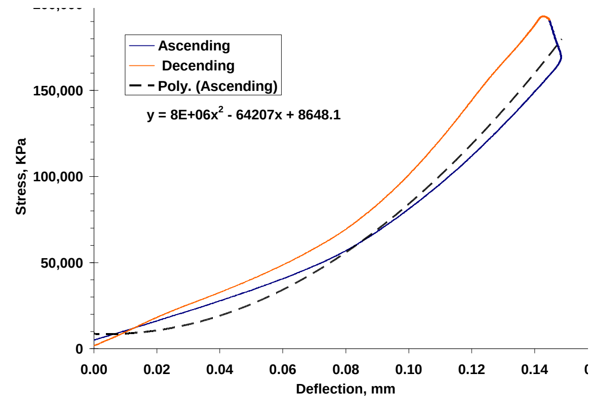

Figure 16 Steeple Stress vs. Deflection Equation Developed from Disk Slot Test Data

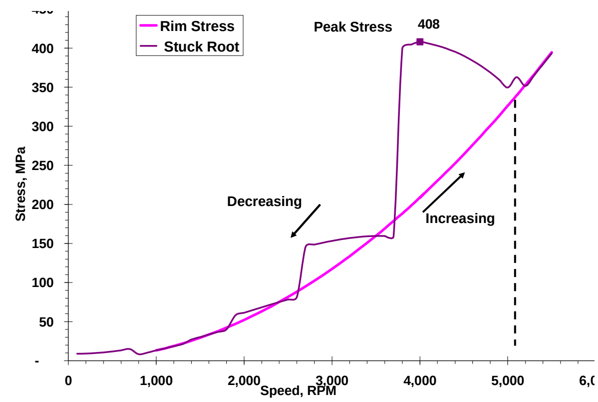

Figure 17 Simulated Blade Root Stress on Shutdown

CONCLUSIONS

- Testing demonstrated that the blade root will stick in the turbine disk slots as load is reduced.
- The coefficients of friction were found to be lower than expected for the blade root tested and the difference between static and sliding friction was small.
- Compared with test data, the rudimentary stick-slip model is reasonably close to the measured load ascension results, but it does not accurately follow the results during load reduction.

- While the model was sufficient to support the premise of this analysis, it is believed that a more realistic simulation could be produced by a numerical model that allows partial slippage across the contact surfaces.
- Simulation of the stick-slip effect combined with conventional rim stress analysis indicates turbine disk peak stress can increase by 20% as rotor speed is reduced. Peak stress was found at 80% speed in the power turbine simulation.
- The turbine bearing surfaces appear as little islands of oxide that could interact to preferentially prevent sliding; the fan disk exhibited signs of galling and fretting. These effects are expected to increase friction coefficient with time which may result in further increases in disk stresses.
- There was no attempt to match the blade with the slot from which it came; thus, the asperities would not interact to increase friction during the test. Reduced friction could also be due because the test parts were handled and lubricated in the process of machining.
- Blade root bearing stress (150 kN) is well above the 30 kN galling threshold for most stainless materials; galling would result in higher friction coefficient.
- As the slot stresses only rise above their normal condition for a brief period on shutdown, this rise will not affect creep life of the turbine disk, but this rise can shorten disk life due to LCF or hold time fatigue.
- Rapid speed changes of a high performance jet engine could be significant in introducing greater stress range than expected, which may contribute to the premature low cycle fatigue failures experienced.

ACKNOWLEDGMENT

The authors would like to acknowledge the contributions of Mr. James Feiger, Sr. Research Engineer and Mr. Wally Robeldo, Laboratory Manager, (Both of SwRI) for design of the test fixture, establishing test protocol, and conducting the testing.

REFERENCES

1. D.L. Davidson "Damage mechanisms in high cycle fatigue," Final Report to Air Force Office of Scientific Research, Contract F49620-96-C-0037, January 1999.

2. K S Chan, M. P. Enright, H R Simmons, P J Golden, Ramesh Chandra, Alan C. Pentz, “Toward Developing a Probabilistic Methodology for Predicting High-Cycle Fretting Fatigue in Aero-Engines” Proceedings of ASME TURBOEXPO 2010, GT2010-23007, Glasgow, Scotland.

3. M. P. Enright, K S Chan, J P Moody, P J Golden, Ramesh Chandra, Alan C. Pentz, “Probabilistic Fretting Fatigue Assessment of Aircraft Engine Disks”, J Engineering for Gas Turbines and Power, January 2010, Vol. 132, ASME

4. H. Murphy, G Harish, T N Farris, “Efficient Modeling of Fretting of Disk/Blade Contacts Including Load History Effects”, J of Tribology, Vol. 126, January 2004, Trans of ASME

5. R.E. Dundas "Design of the gas turbine," in Sawyer's Gas Turbine Engineering Handbook, Second Edition, J.W. Sawyer, ed., Vol. I, pp. 79-150, Gas Turbine Publications, Stamford, CT 06904, 1972

6. Aeronautical Vest-Pocket Handbook, Pratt & Whitney Aircraft, January 1964

7. Jane's All the World's Aircraft

8. G.B. Sinclair and N.G. Cormier "Contact stresses in dovetail attachments: physical modeling," Proceedings of ASME TURBOEXPO 2000, 2000GT-356, ASME, Munich, Germany

9. G.B. Sinclair and N.G. Cormier "Contact stresses in dovetail attachments: alleviation via precision crowning," Proceedings of ASME TURBOEXPO 2001, 2001GT-0550, ASME, New Orleans, LA, USA

10. Timoshenko & Goodier Theory of Elasticity, 3rd Edition, Mcgraw Hill (1970)